Published OnlineFirst December 19, 2013; DOI: 10.1158/0008-5472.CAN-13-2921-T

Cancer Research

High Fidelity Patient-Derived Xenografts for Accelerating Prostate Cancer Discovery and Drug Development

Dong Lin, Alexander W. Wyatt, Hui Xue, et al.

Cancer Res 2014;74:1272-1283. Published OnlineFirst December 19, 2013.

Published OnlineFirst December 19, 2013; DOI: 10.1158/0008-5472.CAN-13-2921-T

Tumor and Stem Cell Biology

Cancer Research

High Fidelity Patient-Derived Xenografts for Accelerating Prostate Cancer Discovery and Drug Development

Dong Lin[1,2,3], Alexander W. Wyatt[1,2], Hui Xue[3], Yuwei Wang[3], Xin Dong[3], Anne Haegert[1,2], Rebecca Wu[3], Sonal Brahmbhatt[1,2], Fan Mo[1,2], Lina Jong[1,2], Robert H. Bell[1,2], Shawn Anderson[1,2], Antonio Hurtado-Coll[1,2], Ladan Fazli[1,2], Manju Sharma[1,2], Himisha Beltran[5], Mark Rubin[6], Michael Cox[1,2], Peter W. Gout[3], James Morris[4], Larry Goldenberg[2], Stanislav V. Volik[1,2], Martin E. Gleave[1,2], Colin C. Collins[1,2], and Yuzhuo Wang[1,2,3]

Abstract

Standardized and reproducible preclinical models that recapitulate the dynamics of prostate cancer are urgently needed. We established a bank of transplantable patient-derived prostate cancer xenografts that capture the biologic and molecular heterogeneity currently confounding prognostication and therapy development. Xenografts preserved the histopathology, genome architecture, and global gene expression of donor tumors. Moreover, their aggressiveness matched patient observations, and their response to androgen withdrawal correlated with tumor subtype. The panel includes the first xenografts generated from needle biopsy tissue obtained at diagnosis. This advance was exploited to generate independent xenografts from different sites of a primary site, enabling functional dissection of tumor heterogeneity. Prolonged exposure of adenocarcinoma xenografts to androgen withdrawal led to castration-resistant prostate cancer, including the first-in-field model of complete transdifferentiation into lethal neuroendocrine prostate cancer. Further analysis of this model supports the hypothesis that neuroendocrine prostate cancer can evolve directly from adenocarcinoma via an adaptive response and yielded a set of genes potentially involved in neuroendocrine transdifferentiation. We predict that these next-generation models will be transformative for advancing mechanistic understanding of disease progression, response to therapy, and personalized oncology. *Cancer Res; 74(4); 1272–83. ©2013 AACR.*

Introduction

Globally, prostate cancer is the second most commonly diagnosed cancer in men and accounts for 250,000 deaths annually (1). Although androgen deprivation therapy elicits rapid remission, tumors inevitably return as castrate-resistant prostate cancer (CRPC), which often remains androgen-dependent and is essentially untreatable (2). The development of novel therapeutics has been hampered in part through high clinical and biologic heterogeneity and the lack of distinguishable histologic subtypes. However, the age of next-generation sequencing and integrated genomics is providing increasing evidence for molecularly defined subtypes. Although strict correlation with clinical outcome remains elusive, tumors can now be classified by their genome copy number, fusion gene profiles, mutational landscapes, and even mRNA splicing patterns (3–7). To exploit emergent discoveries for mechanistic understanding and therapeutic advances, focus must now turn to the development of a new generation of preclinical models that capture the "omic" diversity of prostate cancer.

Preclinical cancer models for *in vivo* drug tests are commonly based on immune-deficient mice carrying subcutaneous prostate cancer cell line xenografts. Unfortunately, these models fail to reproduce the diverse heterogeneity observed in the clinic, partly due to the increased homogeneity of established cell lines after long-term *in vitro* culturing. Furthermore, cell line xenografts rarely possess the tissue architecture of the original cancer specimens from which the cell lines were derived and, consequently, do not accurately represent the complex biochemical and physical interactions between the cancer cells and various components of their microenvironment as found in the original malignancies. Unsurprisingly, therefore, cell line xenografts frequently fail to adequately predict the efficacy of anticancer agents in the clinic (8). Thus, only approximately 5% of potential new anticancer drugs, which have successfully passed *in vivo* tests, have significant efficacy in clinical trials and are approved for clinical usage by the U.S. Food and Drug Administration (9). The cost of these failures is estimated in the range of hundreds of millions of dollars per drug (10).

Authors' Affiliations: [1]Vancouver Prostate Centre; [2]Department of Urologic Sciences, Faculty of Medicine, University of British Columbia; Departments of [3]Experimental Therapeutics and [4]Radiation Oncology, BC Cancer Agency, Vancouver, British Columbia, Canada; Departments of [5]Medicine and [6]Pathology and Laboratory Medicine, Weill Cornell Cancer Center, Weill Cornell Medical College, New York, New York

Note: Supplementary data for this article are available at Cancer Research Online (http://cancerres.aacrjournals.org/).

D. Lin and A.W. Wyatt contributed equally to this work.

Corresponding Authors: Yuzhuo Wang, BC Cancer Agency, 675 West 10th Avenue, Vancouver, BC, Canada VZ5 1L3. Phone: 604-675-8013; Fax: 604-675-8019; E-mail: ywang@bccrc.ca; and Colin C. Collins, ccollins@prostatecentre.com

doi: 10.1158/0008-5472.CAN-13-2921-T

Published OnlineFirst December 19, 2013; DOI: 10.1158/0008-5472.CAN-13-2921-T

In theory, patient-derived cancer tissue xenograft models, based on direct implantation of fresh cancer tissue specimens into immunodeficient mice [e.g., nude, SCID (severe combined immunodeficient) mice], provide the needed clinical relevance. In other cancers, these xenografts retain the cellular heterogeneity, architectural and molecular characteristics of the original cancer, and its microenvironment (11). However, development of prostate cancer tissue xenograft models has been hampered by low success rates, partly due to poor vascularization of the graft site, with engraftment only successful when applied to advanced cancers with high growth rates (e.g., metastatic tumors; refs. 12–14). As such, existing models represent only a small proportion of cancer phenotypes and do not recapitulate disease heterogeneity (15, 16).

In contrast with the subcutaneous graft site, the subrenal capsule (SRC) site is highly vascularized and associated with a very high take rate for most intact grafted tissues, including benign human prostate tissue (17, 18). Recently, Lawrence and colleagues have also standardized a protocol for subrenal grafting of recombined localized human prostate epithelial tissue with mouse mesenchyme (19). They demonstrate the remarkable effectiveness of the subrenal site for modeling localized prostate tumors (20). Over the past few years, we have established a novel panel of transplantable patient-derived prostate tumor xenograft models, the Living Tumor Laboratory (LTL) series, from intact primary and metastatic clinical specimens via SRC grafting. Our xenografts retain the histopathologic and molecular characteristics of their original parent tumors and represent several recently emerging molecular subtypes of prostate cancer. Therefore, we present a panel of high-fidelity primary and metastatic prostate cancer models, which accurately recapitulate biologic and molecular heterogeneity. This publicly available resource provides the urgently needed tools to advance mechanistic understanding of disease progression and response to therapy, and delivers clinically relevant model systems for evaluation of preclinical drug efficacy and beyond.

Materials and Methods

Materials and animals

Chemicals, stains, solvents, and solutions were obtained from Sigma-Aldrich Canada Ltd., unless otherwise indicated. Nonobese diabetic (NOD)/SCID mice (NOD.CB17-Prkdcscid/J) were originally purchased from The Jackson Laboratory and were bred in the breeding area of specific pathogen–free (SPF) level facility in the Animal Resource Center (ARC), BC Cancer Research Centre. The breeding colonies were managed by the ARC staff and delivered to experimental housing room after being weaned. The mice used for xenografts were 6-to 8-weeks old. All food, water, and litter were sterilized before use. Temperature (20°C–21°C) and humidity (50%–60%) were controlled. Daily light cycles were 12-hour light and 12-hour dark. Cages were changed fully once or twice a week.

Prostate cancer tissue acquisition

Specimens were obtained from patients following a protocol approved by the Clinical Research Ethics Board of the University of British Columbia (UBC) and the BC Cancer Agency (BCCA). The specimens were examined, sectioned, and selected by pathologists for histologic analysis and xenografting. All patients signed a consent form approved by the Ethics Board (UBC Ethics Board #: H09-01628 and H04-60131; VCHRI #: V09-0320 and V07-0058).

SRC grafting and development of transplantable tumor lines

Within 24 hours of sample arrival, a minor portion of the tumor was fixed for histologic analysis. The remainder of the tumors were cut into small pieces ($1 \times 3 \times 3$ mm^3 in size) and grafted into the SRC of male NOD/SCID mice supplemented with testosterone as previously described (18). After 3 to 6 months of growth (or earlier if required by the health status of the hosts), the animals were sacrificed in a CO_2 chamber for necropsy. Tumors were harvested and regrafted into NOD/SCID mice under the kidney capsules. The rapidly growing tumors (transplantable tumor lines) were consistently maintained by serial SRC transplantation. Static xenograft pieces were maintained by serial transplantation for up to 3 years. At each passage of rapidly growing tumors and at the last passage of static tumors, xenografts were harvested, measured, and fixed for histopathologic analysis. The hosts were sacrificed and examined for metastases of human origin in lymph nodes, lungs, livers, kidneys, spleens, and bones (femur). Animal care and experiments were carried out in accordance with the guidelines of the Canadian Council on Animal Care.

Histopathology and immunohistochemistry

Preparation of paraffin-embedded tissue sections and immunohistochemical analyses were carried out as previously described (21). For histopathology, routine hematoxylin and eosin (H&E) staining was carried out. A rabbit polyclonal anti-AR antibody (Affinity BioReagents), rabbit polyclonal anti-PSA antibody (Dako), rabbit monoclonal anti-PTEN antibody (Cell Signaling Technology) and rabbit monoclonal anti-ERG antibody (Epitomics) were used for immunohistochemistry. Biotinylated anti-rabbit immunoglobulins (IgG) and peroxidase-linked avidin/biotin complex reagents were obtained from Vector Laboratories. Control sections were processed in parallel with rabbit nonimmune IgG (Dako) used at the same concentrations as the primary antibodies.

Copy number and gene expression analysis

For DNA and RNA isolation, patient and xenograft tumor sections were processed as previously described (22). We performed genome copy-number profiling using the Agilent SurePrint G3 Human CGH 4 × 180K and 8 × 60K Microarray platforms. Of note, 0.5 μg of genomic DNA was used for hybridization, according to the manufacturer's standard protocols as previously described (7, 22). Limited sample availability of patient samples 972 and 1,005 prevented array comparative genomic hybridization (aCGH) analysis. Instead, from these 2 patients, we used DNA-Seq–derived copy-number profiles, which were published previously (7). All copy-number profiles were visualized and analyzed using the Biodiscovery Nexus Copy Number software package v6.0. The hierarchical clustering used complete linkage and a Euclidean distance metric.

Published OnlineFirst December 19, 2013; DOI: 10.1158/0008-5472.CAN-13-2921-T

For gene expression, total RNA samples were prepared following Agilent's One-Color Microarray-Based Gene Expression Analysis Low Input Quick Amp Labeling v6.0. An input of 100 ng of total RNA was used to generate cyanine-3–labeled cRNA. Samples were hybridized on Agilent SurePrint G3 Human GE 8 × 60K Microarray (Design ID, 028004). Arrays were scanned with the Agilent DNA Microarray Scanner at a 3-μm scan resolution and data were processed with Agilent Feature Extraction 10.10. Processed signal was quantile normalized with Agilent GeneSpring 11.5.1. Hierarchical clustering of gene expression data was performed using distance metrics calculated from pairwise correlation coefficients. Comparisons between samples were carried out using fold change of expression. Gene Ontology Term Enrichment was performed using DAVID Bioinformatics Resources v6.7 (23). aCGH copy number and microarray gene expression data are available at GEO accession number GSE41193.

Sequence data analysis

Matched whole-genome sequencing (DNA-seq) and transcriptome sequencing (RNA-seq) of LTL331 and LTL331R was performed at the BCCA Michael Smith Genome Sciences Centre according to standard protocols. For analyses of RNA-seq data [including the neuroendocrine prostate cancers (NEPC) clinical cohort; ref. 24], reads were first mapped onto the HG19 genome and exon–exon junctions by splice-aware aligner Tophat, using the known gene model annotation from Ensembl release 62. Reads with an unmapped mate or multimapped location were filtered out using BamTools and PCR or sequencing optical duplicates were marked and removed by Picard. On the basis of the alignment of RNA-seq reads, gene expression profiles for each sample were calculated on the basis of the gene annotation (Ensembl release 62). Only reads that were unique to one gene and exactly corresponded to gene structure were assigned to the corresponding genes. Raw read counts were normalized by R package DESeq across all samples. Adenocarcinoma samples were compared with NEPC samples using fold change in gene expression. Fusion transcripts and associated genomic breakpoints in LTL331 and LTL331R (Supplementary Fig. S8) were identified from RNA-Seq and DNA-Seq using the nFuse algorithm (25). To validate fusion junctions, primers were designed that flanked the predicted fusion position, and PCR reactions were performed to amplify the fusion fragments from cDNA. All amplification products were sequenced with ABI PRISM 310 Genetic Analyzer using standard techniques to confirm identity.

Results

Generation and maintenance of transplantable patient-derived tumor lines

Directly after surgery or biopsy, fresh primary or metastatic prostate cancer samples from 18 patients (collected February 2008 to May 2010) were transplanted into the SRC of male NOD/SCID mice supplemented with testosterone. Tumors from 2 of 18 patients were terminated because of development of B-cell lymphoma (26), whereas 9 of 16 were viable but static for >2 years after grafting. However, tumors from 7 of 18 patients, including five needle biopsy samples from 1 patient, showed robust growth after an initial latency period (time from initial engraftment until tumor volume reaches 100 mm^3) ranging from 3 to 37 months (median, 22 months; Table 1). From these 7 patients, we established and expanded 12 transplantable tumor lines for a minimum of five generations of serial passaging (Table 1; Fig. 1; Fig. 2; Supplementary Fig. S1; www.livingtumorlab.com). Nine transplantable tumor lines were developed from primary tumors (5 different patients). Furthermore, 7 of these lines were derived from needle biopsies (3 different patients), the first-time needle biopsies have been captured in a patient-derived xenograft model, and a significant step forward, given the critical node prostatic biopsies occupy in clinical diagnostic decisions. Small pieces of xenograft tissue (1 mm^3) from all transplantable tumor lines were collected at early generations (e.g., <5 generations) and frozen with dimethyl sulfoxide (DMSO). These stocks are maintained in liquid nitrogen tanks as frozen seeds, and can be recovered in NOD/SCID mice (mean recover rate using SRC grafting was 95%).

The two transplantable tumor lines with the briefest latency before line establishment (3 and 6 months), and the fastest tumor volume doubling time (10–12 days), were derived from metastatic NEPC (Table 1). This is consistent with the clinic, where NEPC is an aggressive histopathologic subtype of prostate cancer for which there is no effective therapy (27). The remaining 10 of 12 transplantable tumor lines represent adenocarcinoma, the dominant histopathologic subtype in the clinic (95% of diagnoses). In adenocarcinoma lines, tumor volume doubling time ranged from 10 to 23 days. Apart from the initial latency period after patient tumor engraftment, once lines were established, there was no latency at each generation of serial transplantation.

Preservation of donor prostate tumor histopathology

All transplantable tumor lines retained the major histopathologic characteristics of their matched patient tumor (Table 1; Fig. 2 and Supplementary Fig. S1). In at least three serial generations of each adenocarcinoma line, we observed conservation of either the glandular structure or solid sheet, depending on the differentiation status of the original patient tumor. Furthermore, each line retained expression of markers of prostatic adenocarcinoma, e.g., androgen receptor (AR) and prostate-specific antigen (PSA). The two xenografts exhibited solid sheets of round/oval tumor cells with minimal cytoplasm and frequent mitotic figures, consistent with clinical NEPC. The lines were negative for AR and PSA expression but positive for the NEPC markers chromogranin A (CHGA) and synaptophysin (SYP). Accordingly, PSA was undetectable in the serum of hosts bearing NEPC lines. In contrast, serum PSA in all adenocarcinoma line hosts broadly corresponded to tumor volume (Supplementary Fig. S2).

Conservation of patient tumor molecular characteristics and prostate cancer heterogeneity

Chromosomal aberration is a sentinel feature of many cancers, and the associated gene deregulation and genome instability is implicated in the development and progression of prostate cancer (5, 6, 28–30). Combined genome copy-number analysis of each independent transplantable tumor line

Published OnlineFirst December 19, 2013; DOI: 10.1158/0008-5472.CAN-13-2921-T

Table 1. Histopathologic and molecular characteristics of LTL xenograft models and corresponding original tumors

	Original tumor information						Transplantable tumor line information									
Tumor line ID	Source	Diagnosis	AR	PSA	SYP	Latency[a] (mo)	Doubling time[b] (d)	Metastasis	Androgen sensitivity	AR	PSA	SYP	SPINK1	ERG	TMPRSS2-ERG	PTEN	*PTEN* gene
LTL310	Primary PCa	AC	+	+	−	37	ND	No	Yes	+	+	−	−	+	ND	−	−/−
LTL311	Primary PCa	AC	+	+	−	14	10	Yes	Yes	+	+	−	−	−	−	−	−/−
LTL331	Primary PCa	AC	+	+	−	17	9	Yes	tNEPC[c]	+	+	−	−	+	+	−	−/−
LTL412	L.N. metastasis	AC	+	+	−	8	16–19	No	Yes	+	+	−	−	−	−	−	+/−
LTL418	Primary PCa	AC	+	+	−	8	17–19	No	Yes	+	+	−	+	−	−	+	+/+
LTL313A	Primary PCa	AC	+	+	−	22	10–14	Yes	Yes	+	+	−	−	+	+	−	−/−
LTL313B	Primary PCa	AC	+	+	−	22	11–20	No	Partial[c]	+	+	−	−	+	+	−	−/−
LTL313C	Primary PCa	AC	+	+	−	22	23	No	Yes	+	+	−	−	+	+	−	−/−
LTL313D	Primary PCa	AC	+	+	−	22	11–15	Yes	Yes	+	+	−	−	+	+	−	−/−
LTL313H	Primary PCa	AC	+	+	−	13	11–13	Yes	Yes	+	+	−	−	+	+	−	−/−
LTL352	Uretheral metastasis	NEPC	−	−	+	3	11	Yes	No	−	−	+	−	−	+	+	−/+
LTL370	Penile metastasis	NEPC	−	−	+	6	13	Yes	No	−	−	+	−	−	+	+	−/+
LTL313BR	LTL313B	AC	+	+	−	N/A	17–18	ND	No	+	+	−	−	+	+	−	−/−
LTL331R	LTL331	AC	+	+	−	N/A	6–8	Yes	No	−	−	+	−	−	+	−	−/−

NOTE: All expression status refers to protein expression unless otherwise stated.

Abbreviations: AC, adenocarcinoma; N/A, not available; ND, not determined; PCa, prostate cancer; tNEPC, treatment-induced transdifferentiation into NEPC.

[a]time taken from initial engraftment until establishment of a transplantable tumor line;

[b]tumor volume doubling time of each transplantable tumor line once established;

[c]relapse after an initial response to castration.

Published OnlineFirst December 19, 2013; DOI: 10.1158/0008-5472.CAN-13-2921-T

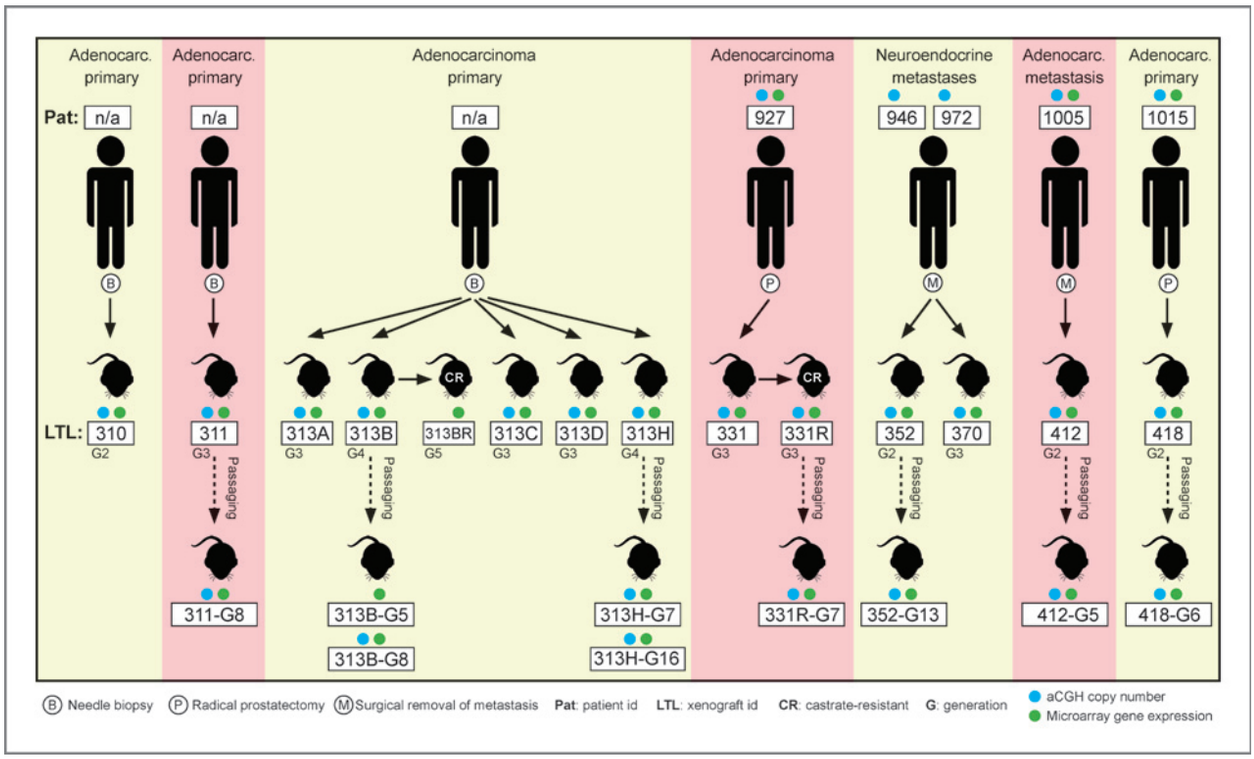

Figure 1. Schematic summary of the transplantable tumor line xenograft models.

demonstrated that they recapitulate both the heterogeneity of prostate cancer and key chromosomal alterations frequently observed (Fig. 3A; refs. 6, 31). For example, in agreement with published patient tumor cohorts, we observed frequent loss of 8p and key tumor suppressors such as *TP53, NKX3-1*, and *RB1*, as well as gains of 8q and oncogenes such as *ETV1, EZH2*, and *BRAF* (Fig. 3A). Six of seven independent tumor lines (11of 12 overall) showed homozygous or heterozygous loss of *PTEN*, which was consistent with PTEN protein expression (Table 1; Fig. 1; Supplementary Fig. S1).

Where comparisons between patient tumor and xenograft were possible ($n = 5$), the chromosomal copy-number profiles

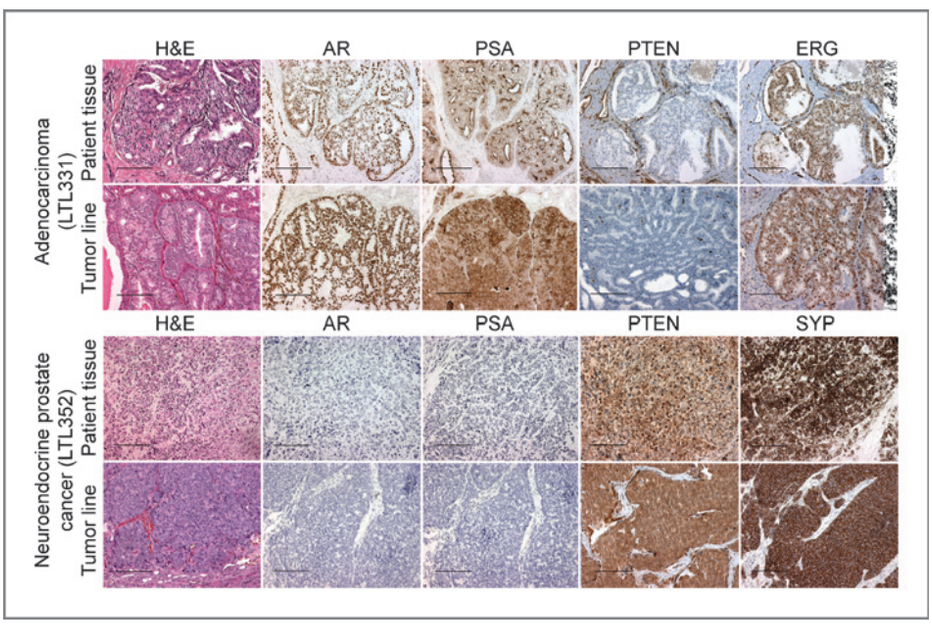

Figure 2. Transplantable tumor lines retain the histolopathologic characteristics of their original patient tumor. Transplantable tumor lines LTL331 and LTL352 show similar tissue structure to the patient tumor from which they were originally derived (H&E stain). Immunohistochemical stains show that the protein expression of key markers (AR, PSA, PTEN, ERG, and SYP) is also conserved. LTL331, adenocarcinoma; LTL352, neuroendocrine prostate tumor. Scale bars, 100 μm.

Published OnlineFirst December 19, 2013; DOI: 10.1158/0008-5472.CAN-13-2921-T

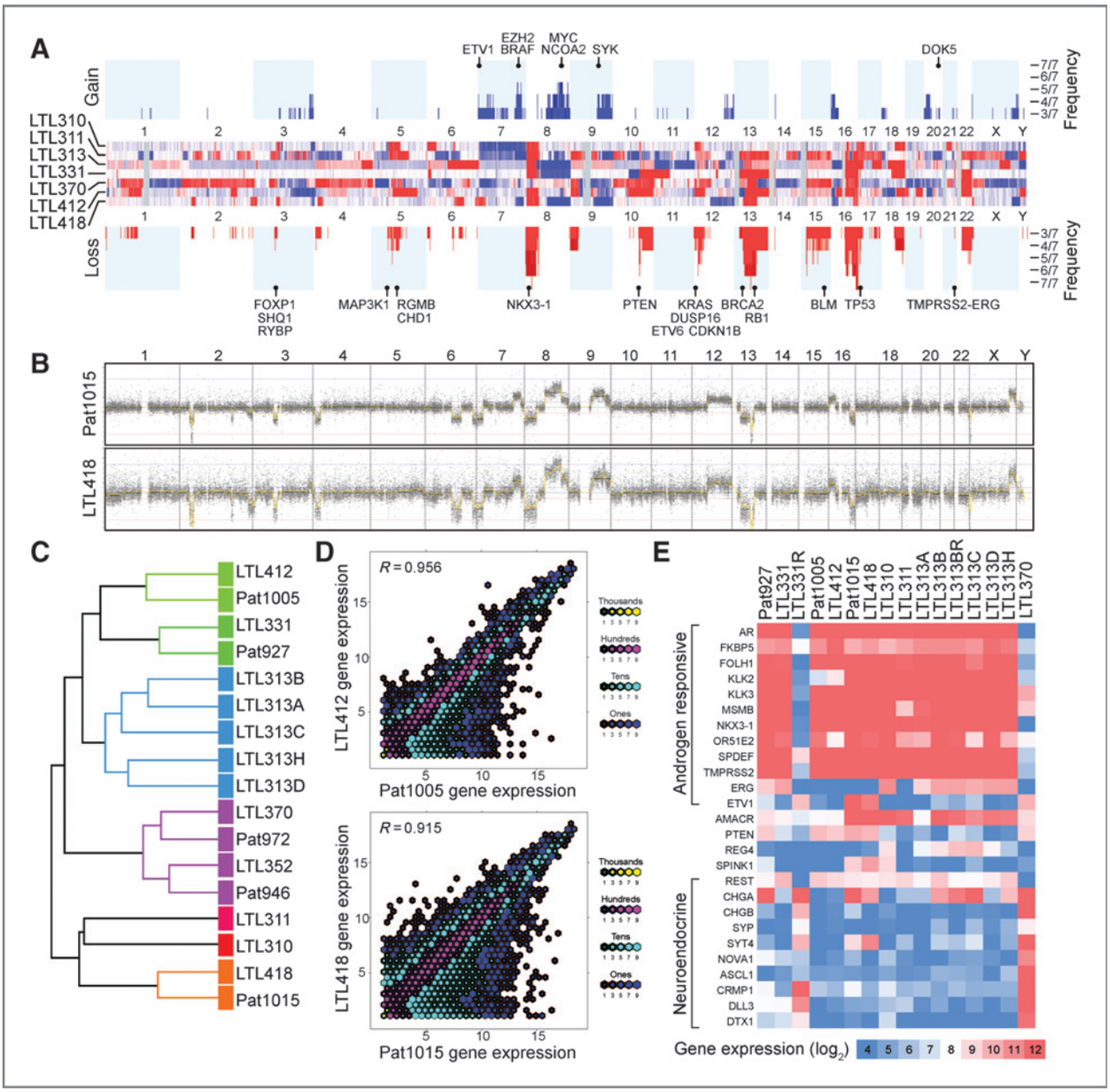

Figure 3. Copy number and gene expression analysis of the xenograft models. A, genome copy-number analysis of each independent transplantable tumor line. Each tumor line is represented by an aCGH-derived heatmap (blue, genomic gain; red, genomic loss). The frequency plots above and below the heatmaps demonstrate aberrations that are shared between multiple lines. Significant cancer genes are annotated. B, example comparison between matched patient 1015 and LTL418, demonstrating the conservation of chromosomal copy-number status. C, unsupervised hierarchical clustering of copy-number profiles demonstrating that each transplantable tumor line is most similar to its original patient tumor. D, hexbin plots illustrating the high correlation of gene expression between xenografts and matched original patient tumors (see also Supplementary Fig. S5). E, heatmap of selected gene expression levels across the transplantable tumor line cohort.

in the transplantable tumor lines closely resembled the original tissues (Fig. 3B; Supplementary Figs. S3 and S4). Unsupervised hierarchical clustering of copy-number segmentation profiles confirmed that all patient and xenograft pairs cluster together, further suggesting conservation of gross genome structure (Fig. 3C). In a recent study, we demonstrated that one of these models (LTL352) retained not just the gross genome structure, but also the expression profile of the parent tumor (7). Consistent with this finding, the transplantable tumor lines with matched patient tumor gene expression demonstrated high conservation of gene expression levels (Fig. 3D; Supplementary Fig. S5).

Gene expression profiling further demonstrated the diversity and heterogeneity captured by the xenograft lines (Fig. 3E). Expression of *TMPRSS2-ERG* marks 20% to 50% of prostate cancer, and is believed to be an early event in carcinogenesis

Published OnlineFirst December 19, 2013; DOI: 10.1158/0008-5472.CAN-13-2921-T

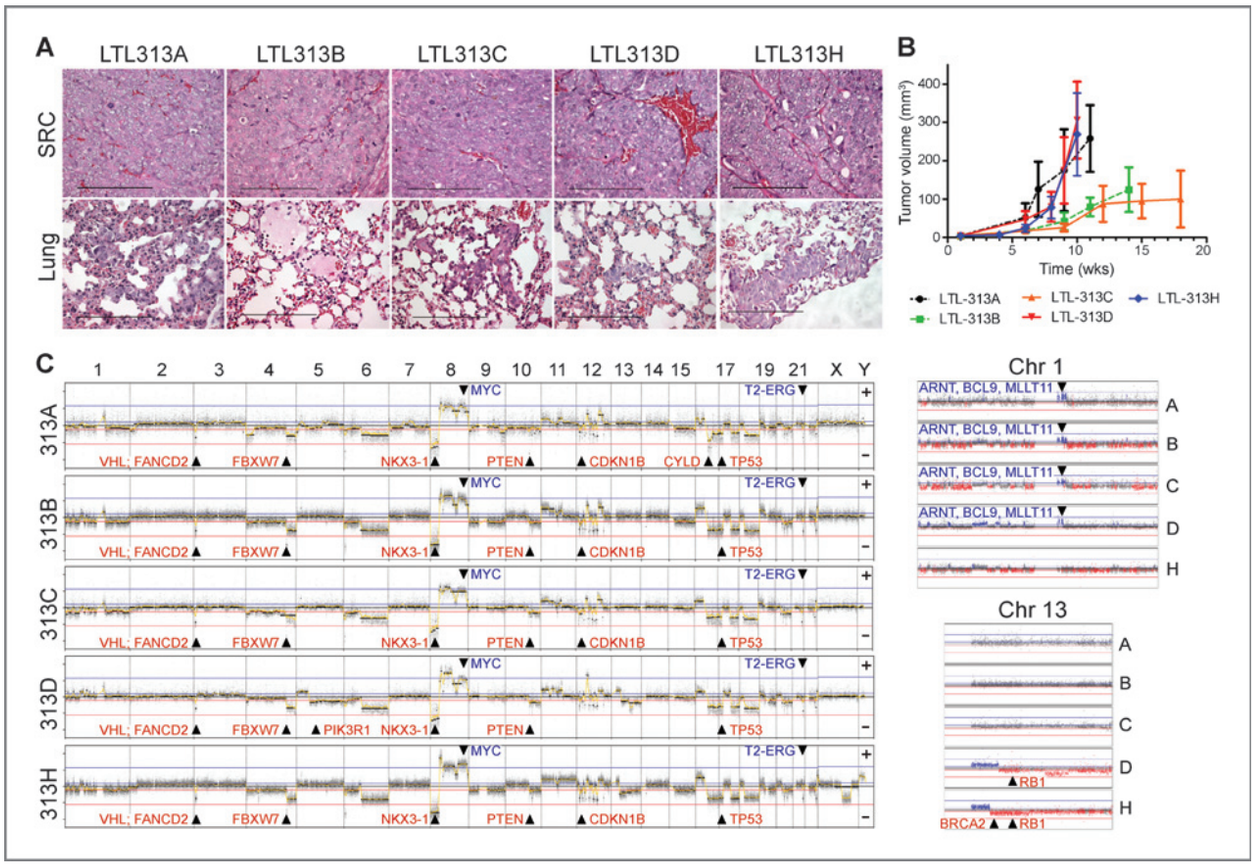

Figure 4. LTL313 xenografts derived from multiple needle biopsies recapitulate functional heterogeneity of primary prostate cancer. A, histopathology of each line demonstrating similar primary tissue structure (top), but different metastatic ability in the host (bottom), as evidenced by representative sections of host lung demonstrating presence or absence of microscopic metastases. Scale bars, 100 μm. B, graph illustrating the different growth rates of the LTL313 lines. C, chromosomal copy-number status in each line showing the similar patterns of aberration, highly suggestive of shared ancestry. Important prostate cancer genes affected by copy-number gain or loss are annotated by arrowheads. Several examples of differences between lines are annotated, including focal variations on chromosomes 1 and 13.

(3, 32–34). Transplantable tumor lines LTL310, LTL331, and LTL313A-H were developed from *TMPRSS2-ERG*–positive tumors and accordingly expressed *TMPRSS2-ERG* at the mRNA level (Fig. 3E) and high levels of ERG at the protein level (Table 1; Fig. 1; Supplementary Fig. S1). NEPC lines LTL352 and LTL370 exhibited an interstitial deletion between *TMPRSS2* and *ERG* (Supplementary Fig. S3), but no ERG expression was detectable, presumably because the androgen responsive gene *TMPRSS2* is no longer under transcriptional pressure. The LTL418 tumor line was *TMPRSS2-ERG* negative, but exhibited high expression of *ETV1* (Fig. 3E), potentially indicating an *ETV1* rearrangement. After ERG, ETV1 is the most common overexpressed ETS gene in prostate tumors. LTL412 and LTL311 were apparently ETS fusion negative. LTL412 was developed from a metastatic tumor, treated for 5 years with antiandrogen therapy, and exhibited clear signs of response to therapy, including expression of constitutive active forms of the AR (7).

Aware of the potential for transplantable tumor lines to evolve after serial passaging in mice and diverge from the original molecular characteristics, we compared copy number and gene expression profiles of late generations with those of the early generations (Supplementary Figs. S4 and S5). After serial passaging, only minimal changes were observed in gross genome copy number. Nevertheless, the preservation of early generations as frozen stock means any divergence can be circumvented if necessary.

Different biopsy foci recapitulate functional heterogeneity

Five of the transplantable tumor lines (LTL313A-H) were derived from needle biopsy specimens from five different foci of a patient's primary tumor (Fig. 4). The slow-to-develop nature of prostate cancer means that at diagnosis a prostate can frequently be colonized by multiple subpopulations of cancer cells, each with potentially different aggressiveness. Understanding this heterogeneity molecularly is of fundamental importance, as critical diagnostic decisions and prognostic predictions are heavily influenced by biopsy. Interestingly, the LTL-313 tumor lines showed different metastatic ability and growth rates *in vivo* (Fig. 4A and B). For example, mice harboring LTL313H reproducibly developed microscopic metastases in the lung (29 of 34 mice), whereas LTL313B exhibited very low metastatic potential (1 of 11 LTL313B mice developed metastases). Copy-number profiling revealed that all five lines shared major

Published OnlineFirst December 19, 2013; DOI: 10.1158/0008-5472.CAN-13-2921-T

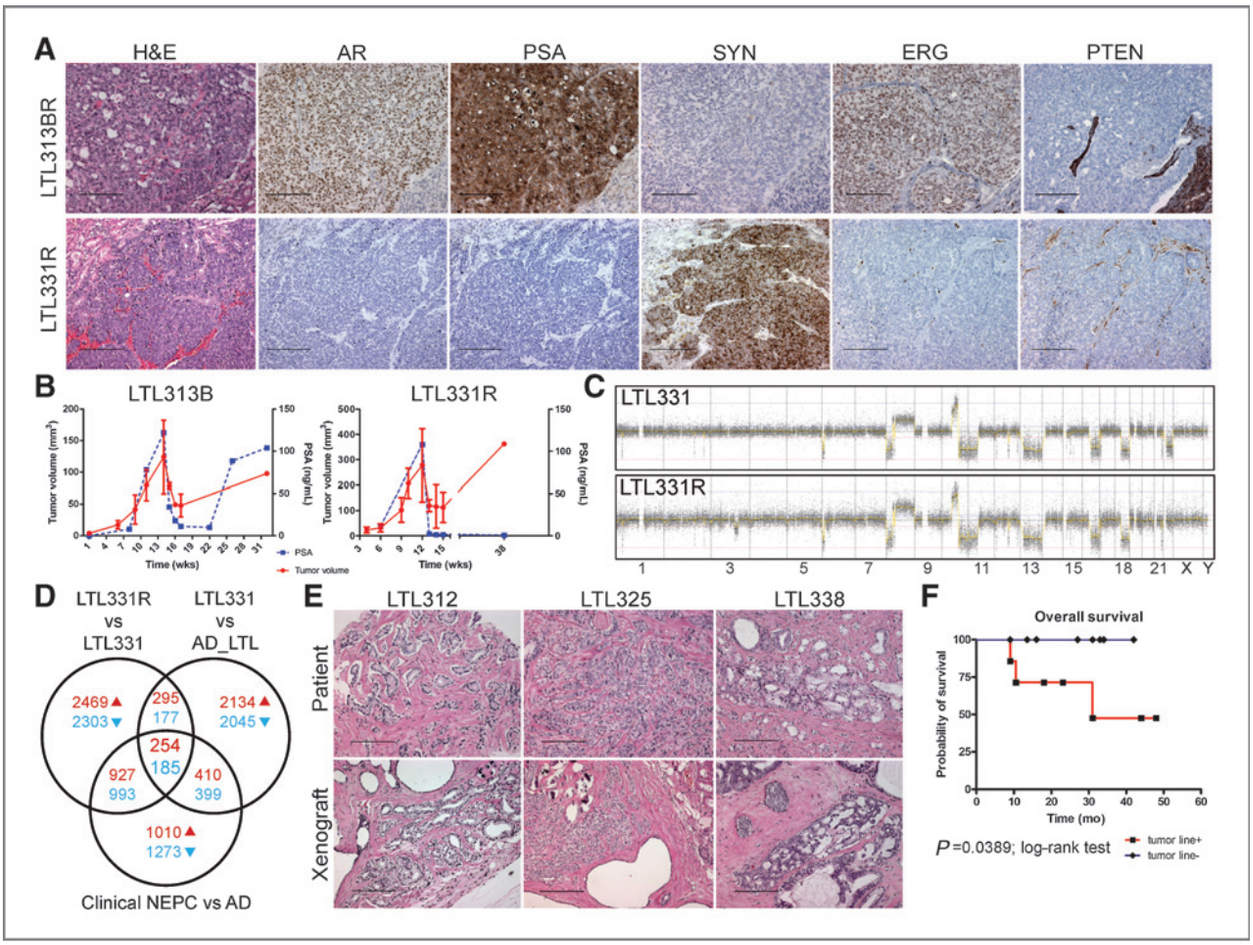

Figure 5. Emergence of CRPC and clinical association of xenografts. A, histopathologic characteristics of castrate-resistant tumors, LTL313BR and LTL331R, showing typical markers of AR-driven adenocarcinoma in LTL313BR but uniform expression of NEPC markers in LTL331R. B, tumor volume and host plasma PSA levels in response to castration. C, copy-number profiles of LTL331 (before castration) and LTL331R (after relapse) demonstrating the high similarity, consistent with neuroendocrine transdifferentiation from adenocarcinoma cells. D, Venn diagram illustrating the intersection between genes up or downregulated in three different comparisons: LTL331 versus LTL331R, LTL331 versus all other adenocarcinoma xenografts (AD_LTL), and NEPC versus adenocarcinoma (AD) patient tumors. E, histopathology of "static" patient-derived xenografts illustrating that the tissue retains original patient tumor histopathologic characteristics after >2 years. F, Kaplan–Meier plot demonstrating a significant difference in overall patient survival between patients whose tumors led to transplantable tumor lines and those whose grafts remained static.

chromosomal alterations, e.g., *PTEN* deletion and *TMPRSS2-ERG* interstitial deletion, and exhibited a broadly similar pattern of aberration, suggesting all lines share a common ancestor (Fig. 4B and C; Table 1). However, several unique chromosomal alterations were only observed in particular tumor lines, including for example, deletion of *BRCA2* and *RB1* in LTL313H (Fig. 4C). Therefore, despite the likely monoclonal origin of each biopsy foci, during the colonization of the prostate by the predominant clone, individual populations diverged, creating a series of functionally heterogeneous subpopulations, which are represented by LTL313A-H.

Response to androgen deprivation is consistent with the clinic and leads to the development of CRPC

Because androgen deprivation can lead to CRPC in patients, we examined the response of tumor lines to host castration and bicalutamide treatment (a front-line therapy in the clinic). Host castration resulted initially in a dramatic drop in tumor volume and PSA levels of all adenocarcinoma line hosts, whereas NEPC lines continued to grow in the absence of androgen (Supplementary Fig. S2A). Bicalutamide treatment also resulted in a drop of tumor volume in all adenocarcinoma lines tested; a clinically relevant finding, given almost all patients respond initially to this therapy (Supplementary Fig. S2B; Supplementary Table S1). In LTL313B and LTL331, we observed reproducible castrate-resistant growth (LTL313BR and LTL331R) after several months postcastration (Fig. 5A–C; Supplementary Fig. S6). LTL313BR retained protein expression of AR and PSA, therefore representing the majority of clinical cases in which CRPC remains dependent on AR signaling. However, androgen deprivation can also lead to the development of NEPC; it is estimated that up to 100% of CRPCs have a NEPC component (35). Although, histologically and molecularly, LTL331 is a typical adenocarcinoma, LTL331R was

Published OnlineFirst December 19, 2013; DOI: 10.1158/0008-5472.CAN-13-2921-T

entirely AR- and PSA-negative and uniformly expressed a range of neuroendocrine markers including SYP, CHGA, CHGB, and CD56 (Fig. 3E; Fig. 5A; Supplementary Fig. S6). LTL331R retained its neuroendocrine phenotype and androgen-independent growth when regrafted into either intact, testosterone-supplemented or castrated hosts, which suggested a stable and irreversible transformation (Supplementary Fig. S6). We performed RNA and DNA sequencing of LTL331 and LTL331R. At the gene expression level, LTL331R was highly similar to clinical NEPC tumors, with upregulated genes, including a broad spectrum of neuronal transcription factors, membrane ion channels, receptors, and secreted peptides (Supplementary Fig. S7). Both LTL331 and LTL331R exhibited very similar copy-number profiles (Fig. 5C), and all fusion genes expressed in LTL331 were also identified in LTL331R, with the exception of TMPRSS2-ERG (lost due to the absence of AR expression; Supplementary Fig. S8). These data, together with the absence of NEPC cells in LTL331 precastration (Supplementary Fig. S8), indicate an adaptive response of the major population of adenocarcinoma cells rather than clonal selection of existing NEPC cells. The transformation seems to represent neuroendocrine transdifferentiation, in which NEPC evolves directly from adenocarcinoma cells (36, 37).

Hypothesizing that LTL331 may be "predisposed" to transdifferentiate, we identified 549 upregulated and 362 downregulated genes in our microarray data whose expression were altered in LTL331 relative to other adenocarcinoma xenografts and concomitantly altered in the same direction in the NEPC LTL331R (Fig. 5D; Supplementary Fig. S9). We compared this list of genes to those showing the same trend in a unique clinical cohort comparing seven NEPC tumors to 30 adenocarcinoma tumors (24). There was a high overlap between the gene lists emerging from xenograft comparisons and the clinical data, further highlighting the fidelity of our models, with 254 up and 185 downregulated genes shared (Fig. 5D; Supplementary Table S2). The upregulated signature was highly enriched for genes involved in neuron differentiation (GO, 0030182; Benjamini–Hochberg corrected $P = 4.4 \times 10^{-5}$), and included key regulatory genes such as *MYT1, PROX1, DPYSL5, APLP1, CELSR3, WDR62, UHRF1*, and *MYBL2*. Evaluation of these genes in another independent clinical cohort of 216 adenocarcinoma cases with significant follow-up (6) demonstrated that they show altered expression in <10% of cases and association with poor outcome, consistent with the low incidence and lethality of NEPC in the clinic (Supplementary Fig. S9). Importantly, this set of genes was not consistently coexpressed with known neuroendocrine markers, suggesting that their differential expression may not originate from NEPC foci in adenocarcinoma tissue.

Xenografts are associated with clinical outcome and provide retrospective prognostic information

Despite successful establishment of 12 lines from 7 different patients, tumors from 9 of 16 of the original patients failed to exhibit significant growth after 2.5 years of serial passaging in mice. These "static" xenografts still exhibited healthy and viable tissue (Fig. 5E), suggesting tumor quiescence. To our knowledge, the survival of healthy human tissue in the absence of growth for this length of time is quite unprecedented and highlights the remarkable fidelity of the SRC grafting process. Interestingly, the failure or success of xenograft line development provided retrospective prognostic information (Supplementary Table S3). First, only 2 of 9 of the patients whose grafted tumors remained static had a PSA recurrence, compared with all (7 of 7) whose tumors led to successful xenograft line development ($P = 0.0032$, Fisher exact test). Second, the patients whose grafts developed into transplantable tumor lines demonstrated poorer overall survival compared with those whose grafts were static ($P = 0.0389$, log-rank test; Fig. 5F). Finally, we also observed that within the LTL panel, latency brevity before tumor line development was significantly correlated with time to PSA recurrence in the patient ($r^2 = 0.83$; $P = 0.0044$; Supplementary Fig. S2C).

Discussion

We have established a bank of transplantable patient-derived prostate tumor xenograft models that, for the first time, capture the diverse heterogeneity of primary prostate cancer. Our work showed that (i) SRC grafting of intact prostate tumors yields a very high success rate of tumor line development; (ii) it is possible to generate transplantable tumor lines from primary prostate tumors and even from needle biopsy specimens; (iii) the lines retained salient features of the original patient tumors, including histopathology, clinical marker expression, chromosomal aberration, gene expression profiles, and tumor aggressiveness; (iv) the lines span major histopathologic and molecular subtypes of prostate cancer, capturing the diverse heterogeneity observed in the clinic for the first time; (v) host castration elicited a varied response, including progression to AR-dependent CRPC and neuroendocrine transdifferentiation; and (vi) success of tumor line development provides potential prognostic information for disease recurrence.

Although we, and others, have previously established the advantage of SRC grafting over traditional subcutaneous sites (19), previous reports focussed on the first generation of grafts with relatively short observation time, e.g., 3 months (18, 38, 39). As such, transplantable tumor lines, akin to those presented here, were not developed. One of the major advantages of SRC grafting over traditional subcutaneous grafting is the high tumor take rate (94%) and success rate of transplantable tumor line development (44%); largely due to the vascularization of the kidney (40, 41). The abundant supply of nutrients, hormones, growth factors, and oxygen to transplanted cells and tissues (before they become vascularized) at the SRC site is likely instrumental to the success of the engraftment, and the conservation of patient tumor properties (42–44). The only property that we did not observe in our models is the propensity of clinical prostate tumors to metastasize to the bone. This is probably due to the difference in bone marrow microenvironment between human and mouse (45, 46).

Intratumoral heterogeneity within clinical samples presents significant difficulties for researchers attempting to functionally dissect cancer biology. For example, it has been reported

Published OnlineFirst December 19, 2013; DOI: 10.1158/0008-5472.CAN-13-2921-T

that lethal metastases can arise from one cancer cell precursor (47), but isolating the particular subpopulation most likely to metastasize from within a mixed total population is fraught with challenges. Therefore, our development of multiple transplantable tumor lines (LTL313A-H) from same patient's different primary tumor biopsies provides a next-generation model of intratumoral heterogeneity. Conserved genomic aberrations suggest that these five lines were clonally related, but they exhibited varied metastatic potential, growth rates, and response to castration (development of CRPC in LTL313BR). We anticipate that detailed molecular analyses of these lines will allow an increased understanding of disease progression and the identification of biomarkers for metastasis. Limited successes are beginning to emerge, with the identification of differentially expressed microRNAs (miRNA) between the metastatic and nonmetastatic lines, LTL313B and LTL313H (48).

Success or failure of tumor line development highlights the clinical relevance of our model system. Patients whose grafted tumors developed into transplantable tumor lines had significantly worse clinical outcome than those patients whose grafts remained static. Therefore, the ability of a grafted tumor to grow and thrive within the host seems to be linked to its aggressiveness in the patient, as opposed to experimental variability (a similar observation has been noted in breast cancer xenograft models; ref. 49). Murine stromal infiltration was observed in both the static grafts and the transplantable tumor lines, consistent with previous studies (49, 50) and suggesting that the quiescent state is independent of mouse stroma. It is likely that the static tumors reflect the common clinical scenario in which a proportion of patients have slow-growing cancer, which can be managed through active surveillance. Interestingly, we also observed that latency (the time from initial engraftment to tumor line development) was significantly correlated with matched patients' time to PSA recurrence, providing retrospective prognostic information. All our adenocarcinoma lines respond to androgen withdrawal and bicalutamide treatment, consistent with the clinic where almost all patients initially respond to androgen-withdrawal therapy. A large fraction of patients eventually fail androgen-ablation therapies and relapse with CRPC: a scenario also observed in our models, in which two tumor lines relapsed as CRPC, several months postcastration.

Because CRPC is responsible for the majority of patient deaths, the development of CRPC directly from two hormone-naïve patient-tissue derived lines will be useful for understanding and combating therapy resistance. Furthermore, the complete transformation of adenocarcinoma in LTL331 to uniform NEPC observed in the CRPC LTL331R (in contrast with previously reported xenografts derived directly from clinical NEPC samples; refs. 14, 51), represents that the first time neuroendocrine transdifferentiation has been captured in a preclinical model, and provides strong evidence for epithelial plasticity. Although current therapeutic development focuses on AR-dependent CRPC, there are no targeted treatments for NEPC, and it is hypothesized that the emergence of more potent androgen deprivation therapies [e.g., enzalutamide (52) and abiraterone (53)] will increase the incidence of treatment-induced NEPC. Therefore, our unique model of neuroendocrine transdifferentiation provides a valuable tool for studying the mechanisms of NEPC development and developing novel therapeutic avenues. Indeed, the power and fidelity of this model was demonstrated by a gene expression comparison leveraging clinical cohorts, generating a set of genes potentially involved with neuroendocrine transdifferentiation. Continued refinement of the emergent gene set using higher-resolution technologies is undoubtedly necessary, but the potential for their development as novel molecular markers to aid risk stratification and predict therapy response is clear.

First or early-generation xenografts, which closely mimic a patient's cancer, are especially suitable for "personalized oncology," in which the most effective and least toxic chemotherapeutic regimen is chosen for a patient (16, 54, 55). Early-generation SRC grafts feature most, if not all, of the molecular heterogeneity and histologic complexity that exist in a patient's original cancer. Importantly, all transplantable tumor lines are preserved as frozen stocks at early generations, ensuring that cellular characteristics and composition are maintained, and allowing reproducible and reliable results. The ability to successfully develop transplantable tumor lines from patient tumor needle biopsy specimens (LTL310, 311, and 313A-H) is highly clinically relevant. In prostate cancer, biopsies are typically obtained at diagnosis, and with 98% of patients surviving >10 years after diagnosis, the time-frame for personalized oncology based on an understanding of an individual's biopsies is clearly realistic. Needle biopsy specimens are more practical to obtain than prostatectomy samples, and because they are taken before prostatectomy, their analyses buys time to develop appropriate therapeutic strategies if necessary. Furthermore, because we demonstrated that grafted tumor growth was correlated with poor clinical outcome, they may help distinguish aggressive from indolent disease.

Beyond personalized oncology, we anticipate that our transplantable tumor lines will provide models for preclinical drug evaluation. The potential for this is evidenced by two recent studies that used LTL352 in combination with advanced genomic and transcriptomic profiling to identify and test new drug targets (24, 56). Moreover, translational research using LTL313 led to the discovery of an anti-AR small molecule (57) and a drug candidate, OMN54, which has advanced to a phase I clinical trial (ClinicalTrials.gov Identifier: NCT01555242). In recognition that the SRC grafting method is technically more demanding than the widely used subcutaneous method, our models are publicly available to the research community (http://www.livingtumorlab.com). Furthermore, several of the LTL models (e.g., LTL331R and LTL352), once established, can be grafted subcutaneously either from fresh tissue or frozen seeds. Therefore, we anticipate that our panel of xenograft models, covering a number of molecular subtypes, will deliver clinically relevant model systems for the development of novel therapeutic approaches to prostate cancer.

Disclosure of Potential Conflicts of Interest

No potential conflicts of interest were disclosed.

Authors' Contributions

Conception and design: D. Lin, A.W. Wyatt, L. Goldenberg, S.V. Volik, M.E. Gleave, C.C. Collins, Y. Wang

Development of methodology: D. Lin, H. Xue, Y. Wang, M. Sharma, Y. Wang

Acquisition of data (provided animals, acquired and managed patients, provided facilities, etc.): D. Lin, H. Xue, A. Haegert, S. Brahmbhatt, L. Jong, A. Hurtado-Coll, H. Beltran, M. Rubin, J. Morris, L. Goldenberg, S.V. Volik, M.E. Gleave, C.C. Collins, C.C. Collins, Y. Wang

Analysis and interpretation of data (e.g., statistical analysis, biostatistics, computational analysis): D. Lin, A.W. Wyatt, X. Dong, A. Haegert, F. Mo, R.H. Bell, S. Anderson, M. Cox, L. Goldenberg, S.V. Volik, M.E. Gleave, C.C. Collins, Y. Wang

Writing, review, and/or revision of the manuscript: D. Lin, A.W. Wyatt, H. Beltran, M. Cox, P.W. Gout, L. Goldenberg, M.E. Gleave, C.C. Collins, Y. Wang

Administrative, technical, or material support (i.e., reporting or organizing data, constructing databases): D. Lin, R. Wu, S. Brahmbhatt, L. Jong, A. Hurtado-Coll, J. Morris, C.C. Collins

Study supervision: C.C. Collins, Y. Wang

Pathologic Investigation: L. Fazli

Grant Support

This work was supported by the Canadian Institutes of Health Research (Y. Wang), Centres of Excellence for Commercialization and Research (M.E. Gleave), Prostate Cancer Canada (C.C. Collins, Y. Wang), Prostate Cancer Foundation (C.C. Collins, Y. Wang), BC Cancer Foundation (Y. Wang), The Canadian Prostate Cancer Genome Network (C.C. Collins), Coalition to Cure Prostate Cancer Young Investigator Award (A.W. Wyatt), Prostate Cancer Foundation BC (A.W. Wyatt).

The costs of publication of this article were defrayed in part by the payment of page charges. This article must therefore be hereby marked *advertisement* in accordance with 18 U.S.C. Section 1734 solely to indicate this fact.

Received October 10, 2013; revised November 19, 2013; accepted December 10, 2013; published OnlineFirst December 19, 2013.

References

1. Jemal A, Bray F, Center MM, Ferlay J, Ward E, Forman D. Global cancer statistics. CA Cancer J Clin 2011;61:69–90.
2. Attard G, Cooper CS, de Bono JS. Steroid hormone receptors in prostate cancer: a hard habit to break? Cancer Cell 2009;16:458–62.
3. Rubin MA, Maher CA, Chinnaiyan AM. Common gene rearrangements in prostate cancer. J Clin Oncol 2011;29:3659–68.
4. Barbieri CE, Baca SC, Lawrence MS, Demichelis F, Blattner M, Theurillat JP, et al. Exome sequencing identifies recurrent SPOP, FOXA1 and MED12 mutations in prostate cancer. Nat Genet 2012;44:685–9.
5. Grasso CS, Wu YM, Robinson DR, Cao X, Dhanasekaran SM, Khan AP, et al. The mutational landscape of lethal castration-resistant prostate cancer. Nature 2012;487:239–43.
6. Taylor BS, Schultz N, Hieronymus H, Gopalan A, Xiao Y, Carver BS, et al. Integrative genomic profiling of human prostate cancer. Cancer Cell 2010;18:11–22.
7. Lapuk AV, Wu C, Wyatt AW, McPherson A, McConeghy BJ, Brahmbhatt S, et al. From sequence to molecular pathology, and a mechanism driving the neuroendocrine phenotype in prostate cancer. J Pathol 2012;227:286–97.
8. Johnson JI, Decker S, Zaharevitz D, Rubinstein LV, Venditti JM, Schepartz S, et al. Relationships between drug activity in NCI preclinical *in vitro* and *in vivo* models and early clinical trials. Br J Cancer 2001;84:1424–31.
9. Sharpless NE, Depinho RA. The mighty mouse: genetically engineered mouse models in cancer drug development. Nat Rev Drug Discov 2006;5:741–54.
10. DiMasi JA, Grabowski HG. Economics of new oncology drug development. J Clin Oncol 2007;25:209–16.
11. Garber K. From human to mouse and back: 'tumorgraft' models surge in popularity. J Natl Cancer Inst 2009;101:6–8.
12. van Weerden WM, de Ridder CM, Verdaasdonk CL, Romijn JC, van der Kwast TH, Schroder FH, et al. Development of seven new human prostate tumor xenograft models and their histopathological characterization. Am J Pathol 1996;149:1055–62.
13. Klein KA, Reiter RE, Redula J, Moradi H, Zhu XL, Brothman AR, et al. Progression of metastatic human prostate cancer to androgen independence in immunodeficient SCID mice. Nat Med 1997;3:402–8.
14. Eva Corey RLV. Xenograft Models of Human Prostate Cancer. In: Leland W.K., Chung WBI, Jonathan W. Simons, editors. Contemporary Cancer Research: Prostate Cancer: Biology, Genetics, and the New Therapeutics. 2nd ed. Totawa: Humana Press Inc.; 2007.
15. Wang Y, Sudilovsky D, Zhang B, Haughney PC, Rosen MA, Wu DS, et al. A human prostatic epithelial model of hormonal carcinogenesis. Cancer Res 2001;61:6064–72.
16. Rubio-Viqueira B, Hidalgo M. Direct *in vivo* xenograft tumor model for predicting chemotherapeutic drug response in cancer patients. Clin Pharmacol Ther 2009;85:217–21.
17. Staack A, Kassis AP, Olshen A, Wang Y, Wu D, Carroll PR, et al. Quantitation of apoptotic activity following castration in human prostatic tissue *in vivo*. Prostate 2003;54:212–9.
18. Wang Y, Revelo MP, Sudilovsky D, Cao M, Chen WG, Goetz L, et al. Development and characterization of efficient xenograft models for benign and malignant human prostate tissue. Prostate 2005;64:149–59.
19. Lawrence MG, Taylor RA, Toivanen R, Pedersen J, Norden S, Pook DW, et al. A preclinical xenograft model of prostate cancer using human tumors. Nat Protoc 2013;8:836–48.
20. Toivanen R, Frydenberg M, Murphy D, Pedersen J, Ryan A, Pook D, et al. A preclinical xenograft model identifies castration-tolerant cancer-repopulating cells in localized prostate tumors. Sci Transl Med 2013;5:187ra71.
21. Lin D, Watahiki A, Bayani J, Zhang F, Liu L, Ling V, et al. ASAP1, a gene at 8q24, is associated with prostate cancer metastasis. Cancer Res 2008;68:4352–9.
22. Wu C, Wyatt AW, Lapuk AV, McPherson A, McConeghy BJ, Bell RH, et al. Integrated genome and transcriptome sequencing identifies a novel form of hybrid and aggressive prostate cancer. J Pathol 2012;227:53–61.
23. Huang da W, Sherman BT, Lempicki RA. Systematic and integrative analysis of large gene lists using DAVID bioinformatics resources. Nat Protoc 2009;4:44–57.
24. Beltran H, Rickman DS, Park K, Chae SS, Sboner A, MacDonald TY, et al. Molecular characterization of neuroendocrine prostate cancer and identification of new drug targets. Cancer Discov 2011;1:487–95.
25. McPherson A, Wu C, Wyatt AW, Shah S, Collins C, Sahinalp SC. nFuse: discovery of complex genomic rearrangements in cancer using high-throughput sequencing. Genome Res 2012;22:2250–61.
26. Rowe M, Young LS, Crocker J, Stokes H, Henderson S, Rickinson AB. Epstein-Barr virus (EBV)-associated lymphoproliferative disease in the SCID mouse model: implications for the pathogenesis of EBV-positive lymphomas in man. J Exp Med 1991;173:147–58.
27. Palmgren JS, Karavadia SS, Wakefield MR. Unusual and underappreciated: small cell carcinoma of the prostate. Semin Oncol 2007;34:22–9.
28. Berger MF, Lawrence MS, Demichelis F, Drier Y, Cibulskis K, Sivachenko AY, et al. The genomic complexity of primary human prostate cancer. Nature 2011;470:214–20.
29. Volik S, Raphael BJ, Huang G, Stratton MR, Bignel G, Murnane J, et al. Decoding the fine-scale structure of a breast cancer genome and transcriptome. Genome Res 2006;16:394–404.
30. Raphael BJ, Volik S, Yu P, Wu C, Huang G, Linardopoulou EV, et al. A sequence-based survey of the complex structural organization of tumor genomes. Genome Biol 2008;9:R59.
31. Friedlander TW, Roy R, Tomlins SA, Ngo VT, Kobayashi Y, Azameera A, et al. Common structural and epigenetic changes in the genome of castration-resistant prostate cancer. Cancer Res 2012;72:616–25.
32. Tomlins SA, Rhodes DR, Perner S, Dhanasekaran SM, Mehra R, Sun XW, et al. Recurrent fusion of TMPRSS2 and ETS transcription factor genes in prostate cancer. Science 2005;310:644–8.

Published OnlineFirst December 19, 2013; DOI: 10.1158/0008-5472.CAN-13-2921-T

33. Perner S, Mosquera JM, Demichelis F, Hofer MD, Paris PL, Simko J, et al. TMPRSS2-ERG fusion prostate cancer: an early molecular event associated with invasion. Am J Surg Pathol 2007;31:882–8.
34. Carver BS, Tran J, Gopalan A, Chen Z, Shaikh S, Carracedo A, et al. Aberrant ERG expression cooperates with loss of PTEN to promote cancer progression in the prostate. Nat Genet 2009;41:619–24.
35. Nelson EC, Cambio AJ, Yang JC, Ok JH, Lara PN Jr, Evans CP. Clinical implications of neuroendocrine differentiation in prostate cancer. Prostate Cancer Prostatic Dis 2007;10:6–14.
36. Williamson SR, Zhang S, Yao JL, Huang J, Lopez-Beltran A, Shen S, et al. ERG-TMPRSS2 rearrangement is shared by concurrent prostatic adenocarcinoma and prostatic small cell carcinoma and absent in small cell carcinoma of the urinary bladder: evidence supporting monoclonal origin. Mod Pathol 2011;24:1120–7.
37. Lotan TL, Gupta NS, Wang W, Toubaji A, Haffner MC, Chaux A, et al. ERG gene rearrangements are common in prostatic small cell carcinomas. Mod Pathol 2011;24:820–8.
38. Priolo C, Agostini M, Vena N, Ligon AH, Fiorentino M, Shin E, et al. Establishment and genomic characterization of mouse xenografts of human primary prostate tumors. Am J Pathol 2010;176:1901–13.
39. Zhao H, Nolley R, Chen Z, Peehl DM. Tissue slice grafts: an *in vivo* model of human prostate androgen signaling. Am J Pathol 2010; 177:229–39.
40. Ott CE, Knox FG. Tissue pressures and fluid dynamics in the kidney. Fed Proc 1976;35:1872–5.
41. Pinter G. Renal lymph: vital for the kidney and valuable for the physiologist. Physiology 1988;3:189–93.
42. Tunstead JR, Thomas M, Hornsby PJ. Early events in the formation of a tissue structure from dispersed bovine adrenocortical cells following transplantation into scid mice. J Mol Med 1999;77:666–76.
43. Cunha GR. Epithelial-stromal interactions in development of the urogenital tract. Int Rev Cytol 1976;47:137–94.
44. Griffin TW, Bogden AE, Reich SD, Antonelli D, Hunter RE, Ward A, et al. Initial clinical trials of the subrenal capsule assay as a predictor of tumor response to chemotherapy. Cancer 1983;52:2185–92.
45. Nemeth JA, Harb JF, Barroso U Jr, He Z, Grignon DJ, Cher ML. Severe combined immunodeficient-hu model of human prostate cancer metastasis to human bone. Cancer Res 1999;59:1987–93.
46. Yonou H, Yokose T, Kamijo T, Kanomata N, Hasebe T, Nagai K, et al. Establishment of a novel species- and tissue-specific metastasis model of human prostate cancer in humanized non-obese diabetic/severe combined immunodeficient mice engrafted with human adult lung and bone. Cancer Res 2001;61:2177–82.
47. Liu W, Laitinen S, Khan S, Vihinen M, Kowalski J, Yu G, et al. Copy number analysis indicates monoclonal origin of lethal metastatic prostate cancer. Nat Med 2009;15:559–65.
48. Watahiki A, Wang Y, Morris J, Dennis K, O'Dwyer HM, Gleave M, et al. MicroRNAs associated with metastatic prostate cancer. PLoS ONE 2011;6:e24950.
49. DeRose YS, Wang G, Lin YC, Bernard PS, Buys SS, Ebbert MT, et al. Tumor grafts derived from women with breast cancer authentically reflect tumor pathology, growth, metastasis and disease outcomes. Nat Med 2011;17:1514–20.
50. Cutz JC, Guan J, Bayani J, Yoshimoto M, Xue H, Sutcliffe M, et al. Establishment in severe combined immunodeficiency mice of subrenal capsule xenografts and transplantable tumor lines from a variety of primary human lung cancers: potential models for studying tumor progression-related changes. Clin Cancer Res 2006;12: 4043–54.
51. Tzelepi V, Zhang J, Lu JF, Kleb B, Wu G, Wan X, et al. Modeling a lethal prostate cancer variant with small-cell carcinoma features. Clin Cancer Res 2012;18:666–77.
52. Scher HI, Fizazi K, Saad F, Taplin ME, Sternberg CN, Miller K, et al. Increased survival with enzalutamide in prostate cancer after chemotherapy. N Engl J Med 2012;367:1187–97.
53. Fizazi K, Scher HI, Molina A, Logothetis CJ, Chi KN, Jones RJ, et al. Abiraterone acetate for treatment of metastatic castration-resistant prostate cancer: final overall survival analysis of the COU-AA-301 randomised, double-blind, placebo-controlled phase 3 study. Lancet Oncol 2012;13:983–92.
54. Dong X, Guan J, English JC, Flint J, Yee J, Evans K, et al. Patient-derived first generation xenografts of non-small cell lung cancers: promising tools for predicting drug responses for personalized chemotherapy. Clin Cancer Res 2010;16:1442–51.
55. Kortmann U, McAlpine JN, Xue H, Guan J, Ha G, Tully S, et al. Tumor growth inhibition by olaparib in BRCA2 germline-mutated patient-derived ovarian cancer tissue xenografts. Clin Cancer Res 2011;17: 783–91.
56. Collins CC, Volik SV, Lapuk AV, Wang Y, Gout PW, Wu C, et al. Next generation sequencing of prostate cancer from a patient identifies a deficiency of methylthioadenosine phosphorylase, an exploitable tumor target. Mol Cancer Ther 2012;11:775–83.
57. Andersen RJ, Mawji NR, Wang J, Wang G, Haile S, Myung JK, et al. Regression of castrate-recurrent prostate cancer by a small-molecule inhibitor of the amino-terminus domain of the androgen receptor. Cancer Cell 2010;17:535–46.